# Redefining the Microwave Plasma-Mediated CO2 Reduction Efficiency Limit: The Role of O-CO2 Association

ACS Energy LETTERS

http://pubs.acs.org/journal/aelccp

LETTER

# Redefining the Microwave Plasma-Mediated $CO_2$ Reduction Efficiency Limit: The Role of O–$CO_2$ Association

Alex van de Steeg, Pedro Viegas, Ana Silva, Tom Butterworth, Alexander van Bavel, Joost Smits, Paola Diomede, Mauritius van de Sanden, and Gerard van Rooij*

Cite This: *ACS Energy Lett.* 2021, 6, 2876–2881

Read Online

ACCESS | Metrics & More | Article Recommendations | Supporting Information

**ABSTRACT:** Reduction of $CO_2$ to CO for sustainable fuel production is studied in high-temperature (>3500 K) microwave plasma. Raman scattering and chemical kinetics modeling reveal chemistry rates with spatial resolution that explain previously reported peak energy efficiency values of 50%. The necessary product quenching is established by fast transport in the core, at frequencies of $10^5$ $s^{-1}$, facilitating rapid mass and energy transfer between products and feedstock $CO_2$. Moreover, the resulting chemical nonequilibrium yields additional $CO_2$ dissociation in O–$CO_2$ association, a reaction responsible for up to 45% of CO production. Three different thermal chemistry sets are invoked to qualitatively confirm this picture. It is shown how these lack predictive accuracy in the high gas temperature regime studied, which indicates that new $CO_2$ chemistry rate coefficients are highly desirable. Improving reactor design with the identified enhancement mechanisms in mind can increase efficiency up to the newly defined thermal limit of 70%.

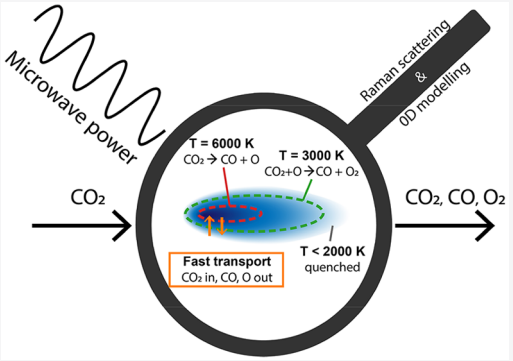


In our transition toward a circular economy, $CO_2$ reduction powered by renewable energy is recognized as an opportunity to produce sustainable carbon feedstocks for the synthesis of fuels and chemicals.[1−3] $CO_2$ reduction with high-temperature microwave plasmas (>3500 K) is a promising technology, as recent experimental results show conversions up to 80% and maximum energy efficiencies up to 50%.[4,5] This maximum experimental energy efficiency is close to the theoretical efficiency limit (∼52%) of thermal $CO_2$ splitting with no CO losses in back-reactions and in which $O_2$ is formed by O-recombination (i.e., with absolute quenching):[4,6,7]

$$CO_2 \rightarrow CO + O \quad \text{(R1)}$$

$$O + O \rightarrow O_2 \quad \text{(R2)}$$

It has been hypothesized that this limit can be increased significantly by controlling the quenching trajectory of the atomic oxygen generated in reaction R1. Association of O with $CO_2$ yields an additional CO for each $O_2$ which, would increase the efficiency limit to 70%[6,8] by valorizing the enthalpy of formation of nascent O atoms:

$$O + CO_2 \rightarrow CO + O_2 \quad \text{(R3)}$$

The mechanism is called superideal quenching,[9,10] but it is yet to be demonstrated to contribute to the overall efficiency. Elucidating the importance of this reaction is the primary goal of this work.

In addition to thermal chemistry, vibrational activation and vibration-driven dissociation is generally assumed to be important in microwave plasmas.[7,9−15] It has been proposed as an explanation for early work with unparalleled energy efficiencies exceeding 80%.[12] However, recent investigations could not link vibrational–translational nonequilibrium with high performance;[8,16−18] instead, in most $CO_2$ microwave plasma experiments, thermal dissociation mechanisms are predominant.[6,8,14,19,20] Nevertheless, it is relevant to note that the vibration-driven mechanism also relies on reaction R3 to complete the reaction scheme with highest efficiency.

Hence, insight into the recombination of O atoms and the potential of its control is decisive for evaluation of the

**Received:** June 11, 2021
**Accepted:** July 19, 2021
**Published:** July 26, 2021

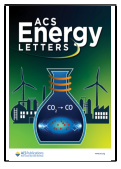

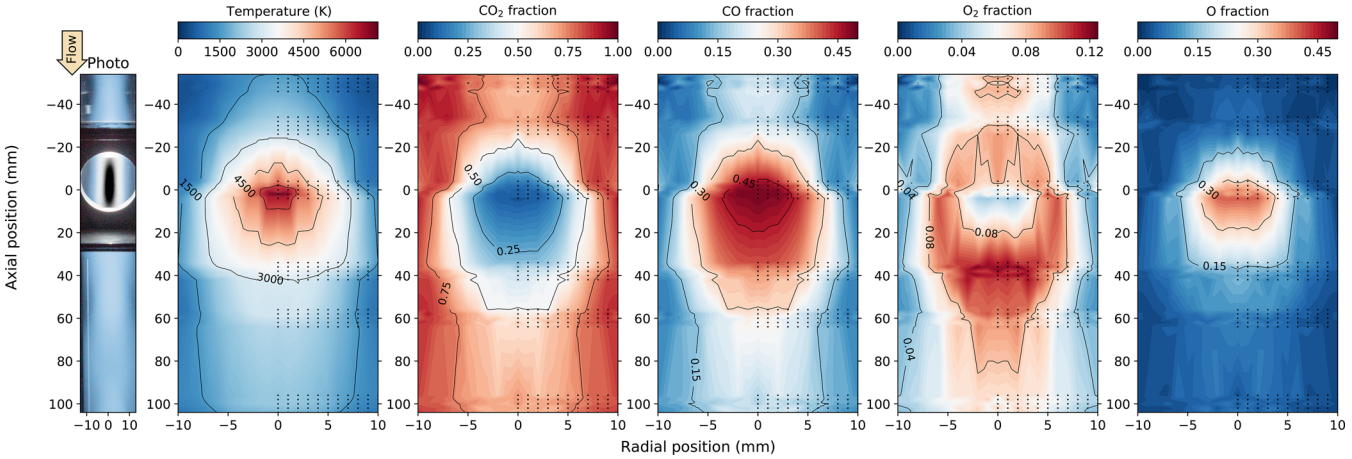


**Figure 1. Plasma emission and spatially resolved Raman results of the 10 slm, 120 mbar, 1000 W plasma. The emission map is an overlay of total emission and 777 nm oxygen emission in the core. Black dots represent locations where Raman spectra are recorded. Cylindrical symmetry is assumed, and data is linearly interpolated between measurement points. Subsequent maps represent rotational temperature, $CO_2$ fraction, CO fraction, $O_2$ fraction, and O fraction.**

maximum performance of $CO_2$ conversion, in microwave plasma in particular, and in high-temperature systems in general. This work succeeds for the first time in unravelling both the quenching mechanisms and reaction kinetics using an *in situ* characterization of the chemical and physical state of the reactor. Raman scattering is used to create maps of temperature (rotational and vibrational)[16] and composition ($CO_2$, CO, $O_2$, and O),[21] with more detail in the Supporting Information. The experimental data is interpreted with our 0D chemical kinetics model[19] to yield local species sources (and sinks). The global reactor productivity is obtained by integrating the local chemistry rates over the volume, which in turn elucidates the importance of O-radical induced $CO_2$ dissociation (reaction R3) compared to the other chemical pathways.

This approach elucidates reaction pathways independent of the unknown flow field in the studied configuration. The rationale is that all locally determined chemical rates sum to the reactor integrated rate of those reactions. We therefore divide the reactor into a fine grid composed of control volumes, in which the effect of complex, local transport phenomena are inherently captured. Notwithstanding this independence of flow in the analysis is the strong dependence of the eventual reactor performance on details of transport and flow, which will affect measured distributions of temperature and composition.

The analysis also relies on accurate knowledge of rate constants. Multiple data sets exist in the literature, and some of their rate constants disagree by several orders of magnitude; the rate constant of the reaction $CO_2 + M \rightarrow CO + O + M$ can differ by an order of magnitude, while that of $O_2$ recombination can vary by 4 orders of magnitude. The most widely used kinetic data are rates (i) from Butylkin,[22] developed at the time of the early experiments and used by, for example, Wolf et al.,[6] Van den Bekerom et al.,[8] and Den Harder et al.;[4] (ii) from GRI-MECH[23] developed for combustion and used by, for example, Viegas et al.;[19] and (iii) derived from the NIST chemical kinetics database, used by, for example, Kozak et al.,[13] Koelman et al.,[11] and Pietanza et al.[24] It is important to note that all sets reasonably approach the equilibrium composition (through Gibbs free energy minimization) at long integration times (see the Supporting Information).

The structure of this Letter is as follows. First, we map rovibrational temperatures and composition in a large cross section of the reactor. Second, this data is used to quantify local chemistry time scales as well as the main reaction pathways of CO production and O-quenching. Thus, we illustrate the potential of superideal quenching to increase energy efficiency in $CO_2$ microwave plasma.

Four experiments featured varying process conditions, with pressures of 60 and 120 mbar and flows of pure $CO_2$ of 10 and 20 slm, all at a fixed input power of 1000 W. The apparent plasma volume decreases with pressure from a diffuse appearance at 60 mbar to a thin and bright filament at 120 mbar because of plasma contraction,[25] an effect that coincides with increasing performance.[4,26] Flow does not affect the plasma shape but changes the quenching trajectory, resulting in improved efficiency. While the precise mechanisms are still unknown, Wolf et al.[6] predicted increasing efficiency with increasing flow is a result of faster downstream cooling.

The Raman-derived temperature and composition measurements (Figure 1) are the basis for the characterization of transport and chemistry. The results illustrate the extreme temperature in which the reactor operates, with the plasma core reaching 6000 K. In this ultrahigh-temperature region, the majority of $CO_2$ is dissociated and CO concentration peaks at 50%. This observation is consistent with the predominance of the thermal $CO_2$ dissociation mechanism. Additionally, $O_2$ is largely absent in the plasma core; instead, atomic oxygen reaches a fraction of almost 50%. Separate regions of O and $O_2$ formation are revealed, and the maxima in these fractions are spatially offset by approximately 40 mm.

The Supporting Information includes results for the other tested conditions. Two main differences are observed with respect to Figure 1. (i) At lower pressure, power absorption is less concentrated; this follows from the broader temperature profile that peaks at a reduced value of 3500−4000 K. Additionally, $CO_2$ is the majority species in the plasma core with concentration fractions above 50% throughout the reactor. (ii) Remarkably, the increased feed gas flow rate results in a larger penetration of products upstream of the plasma core. Consequently, the $O_2$ fraction peaks upstream of


https://doi.org/10.1021/acsenergylett.1c01206
ACS Energy Lett. 2021, 6, 2876−2881

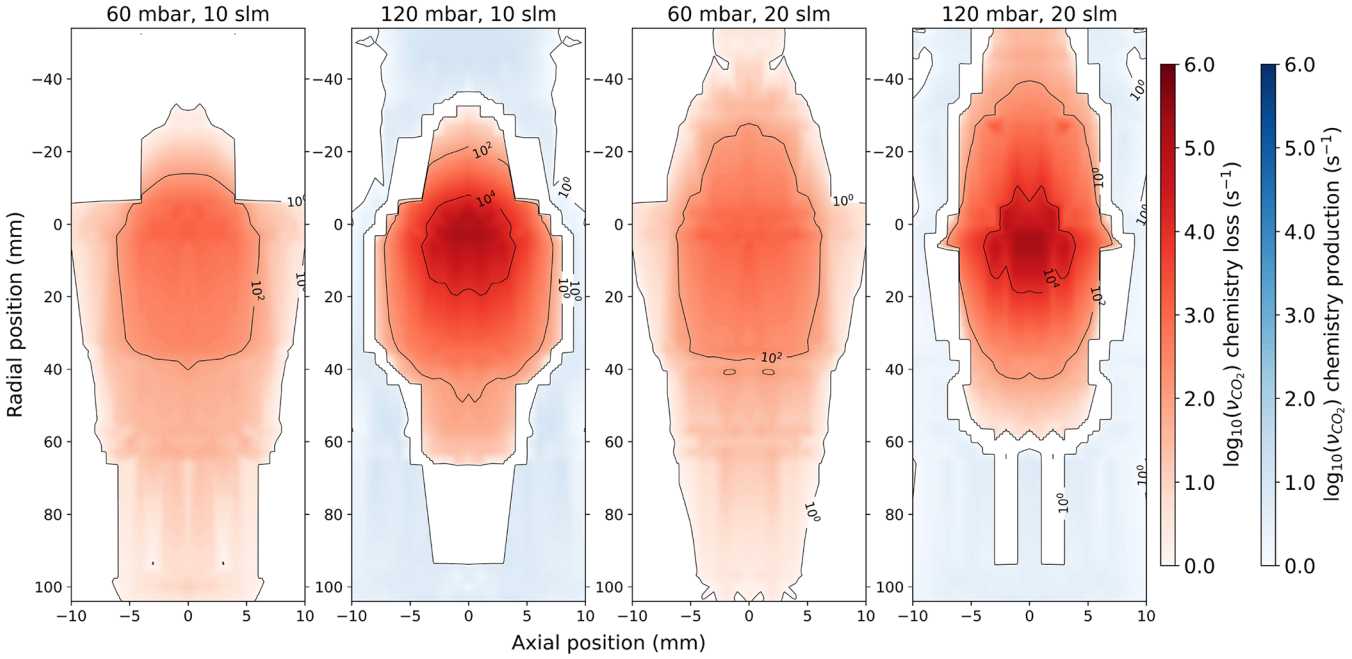


**Figure 2. $CO_2$ replacement frequencies ($\nu_{CO_2}$) for the different discharge conditions as calculated by the plasma chemical kinetics model and GRI-MECH rate constants. Positive chemistry frequencies are shown in blue, and negative transport frequencies are in red. White denotes $-1 < \nu_{CO_2} < 1\ s^{-1}$, where the system is near chemical equilibrium.**

the core instead of downstream. This last finding hints at a flow reversal and recirculation as a result of the tangential gas injection.[6] In the literature, plug-flow behavior is generally assumed in alike configurations,[4,6,8,10,13,20,24,27] which clearly oversimplifies core-exhaust transport.

We have measured vibrational temperatures in several key positions in the reactor via vibrational Raman scattering: a radial scan at 0 mm and at 35 mm for 60 and 120 mbar, 10 slm. Measurements do not show any spectral signature of a vibrational nonequilibrium, neither between the different vibrational modes or with the gas/rotational temperature (see the Supporting Information). It confirms that a Boltzmann distribution can be used to evaluate the rotational and vibrational degrees of freedom.

Although no vibrational nonequilibrium is observed, a strong chemical nonequilibrium is present. For example, the 60 mbar core temperature is ∼4000 K with $CO_2$ as majority species, while chemical equilibrium (often assumed for the core[4,6,28]) shows $CO_2$ fractions below 1% at this temperature. The Supporting Information contains additional details on the present chemical nonequilibrium for the conditions examined. Summarizing, because of the higher temperature, at higher pressure the strongest chemical nonequilibrium is present in the region surrounding the plasma core, while at lower pressure this chemical nonequilibrium occurs within the plasma core.

Deviations from chemical equilibrium are a result of the interplay between fast transport and chemistry. Invoking chemical kinetics modeling allows us to quantify the transport time scales by assuming steady state and a balance between transport and chemistry at each position, for each species $i$:

$$\frac{dn_i}{dt} = 0 = \sum_j S_{i,j} \pm \nu_i n_i \qquad (1)$$

Here $\frac{dn_i}{dt}$ is the temporal derivative of the species number density $n_i$, equal to zero because of the steady-state assumption. $S_{i,j}$ is the chemistry source (or loss, if negative) rate of species $i$ through reaction $j$. The replacement frequency $\nu_i$ of species $i$ is the inverse of the particle transport loss time $t_{ri}$. The $\nu_i n_i$ term can be positive or negative, depending on the sign of the chemistry term, where positive refers to supply of the species.

The chemistry rates $S_{i,j}$ are assessed with our 0D model[19] invoking the three aforementioned thermal chemistry sets. The model also assesses charged particle kinetics assuming an electron density profile that was recently measured in our lab under similar conditions.[25]

Figure 2 shows the spatial distribution of $\nu_{CO_2}$, the transport frequency of $CO_2$, as obtained with the GRI-MECH rate constants, for each pressure and gas flow setting. The Supporting Information discusses the replacement frequency of other particles. The regions where $CO_2$ is formed by chemistry (blue) have a very small chemistry time constant in all conditions, the fastest being of the order of $10^{-1}$ s. This time scale is inconsequential compared with the bulk-transport time scale of the reactor which is 1−2 orders of magnitude shorter.[4,6] In the plasma core, $CO_2$ is supplied by transport and consumed by chemistry (red) with a time scale of $\sim 10^{-5}$ s in the hottest regions. On average, time scales of $10^{-3}$ s at 60 mbar and $10^{-4}$ s at 120 mbar are observed in the plasma core, similar to that described by Wolf et al.[6] Using the Kozak and Butylkin schemes results in slightly different transport values, but the general observations in terms of chemistry remain the same.

The global reactor productivity equals the integration over the local chemistry rates over the total volume. The quenching of O atoms and the different production and loss mechanisms of CO can be directly identified in this way. This analysis is valid only if the complete chemically active portion of the


https://doi.org/10.1021/acsenergylett.1c01206
ACS Energy Lett. 2021, 6, 2876−2881

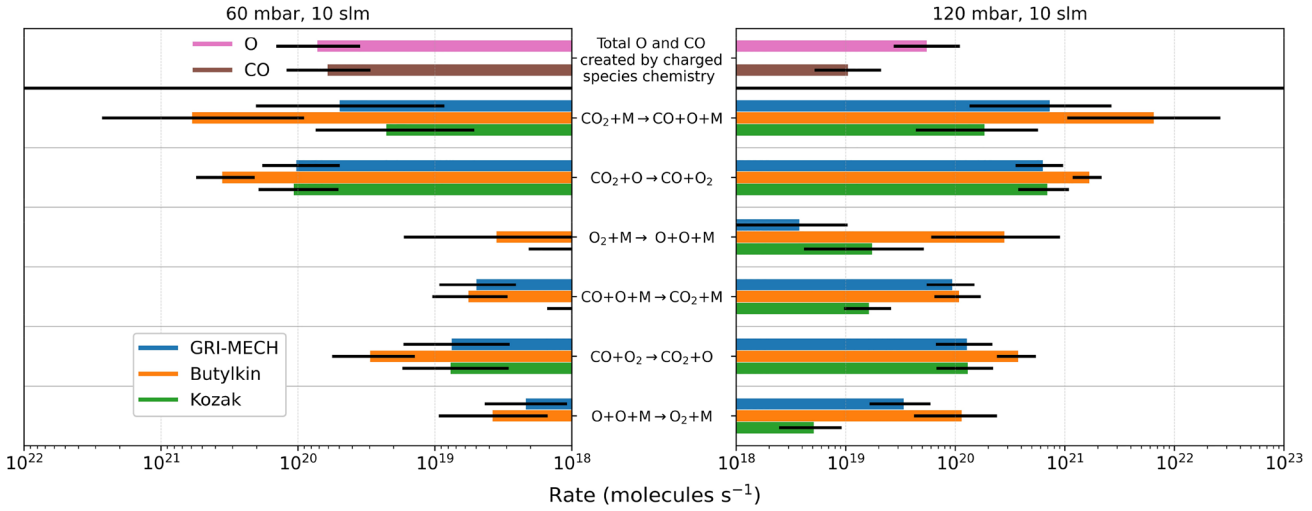


**Figure 3. Reactor integrated rates using three kinetic schemes for low (left) and high (right) pressure. Error margins are propagated from experimental uncertainties in temperature and fractions (see the Supporting Information).**

reactor is captured. Chemistry time scales at $x = -50$ or $x = 100$ mm are $10^{0}$–$10^{-1}$ s, i.e., orders of magnitude lower than in the core or surrounding regions and at least an order of magnitude below average reactor residence times.[4,6] Hence, we conclude there is no notable role of chemistry outside the probed volume. Numerically we calculate the global chemical activity as

$$\frac{dR_{i,tot}}{dt} = \sum_{\bar{x}} \frac{dR_{i,loc}(r, z)}{dt} V(r, z) \tag{2}$$

Here $\frac{dR_{i,tot}}{dt}$ is the reactor integrated rate of reaction $i$, $\frac{dR_{i,loc}(r,z)}{dt}$ the local rate of reaction $i$ at spatial coordinate $(r, z)$, and $V(r, z)$ the volume corresponding to the cylinder element at this coordinate. The reaction rates are calculated over a fine grid using linearly interpolated experimental data.

Figure 3 compares the result for the main reactions and for three chemistry sets. The CO and O production rates through charged species chemistry are plotted separately. Those rates refer to, among others, direct electron impact dissociation, dissociative recombination, and dissociative attachment.

While the absolute rates among the different chemistry sets can vary by more than an order of magnitude, qualitatively all chemistry sets are consistent: back-reactions reforming $CO_2$ are of minimal importance, and charged particle chemistry plays a role in providing dissociation only at low pressure. At higher pressures, thermal chemistry dominates because of contraction, high temperatures, and increasing collisionality. Combining the results of Figure 3 with the locally determined reaction rates elucidates the main dissociation pathways for the 120 mbar conditions: the high-temperature core produces CO and O, while fast transport extracts these and provides fresh $CO_2$. The extracted O atoms then recombine preferentially with $CO_2$ to produce CO and $O_2$; the rate of this reaction is of the same order of magnitude as other CO-producing reactions. These two distinct dissociation reactions are dominant in separate regions: the core, with $T \approx 6000$ K, and surrounding the core, with $T \approx 3000$ K.

While the chemical kinetics sets are all in qualitative agreement, we obtain best quantitative agreement with the GRI-MECH set as shown in Figure 4. In this figure, we compare the total CO production with that measured by

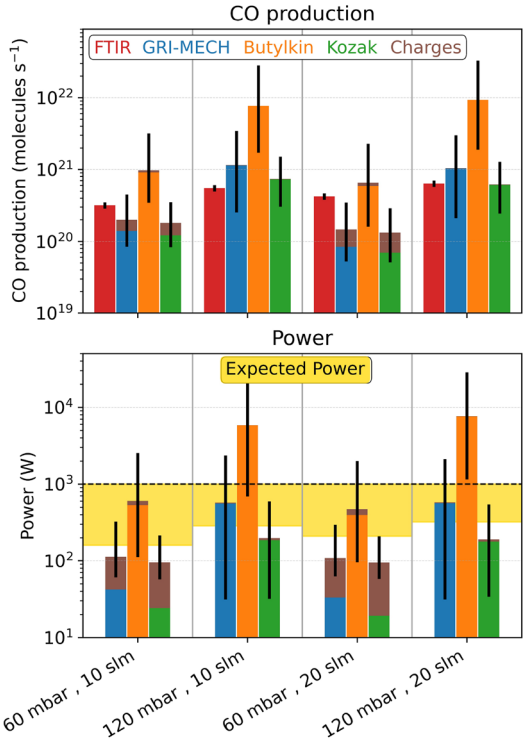


**Figure 4. Comparison of reactor integrated CO production (d[CO]/d$t$) (top) and power consumption (bottom) compared with values measured in the effluent. Error margins are propagated from errors in reaction rates of Figure 3. Power is expected to be in the yellow area, which is between the total input power (1 kW) and the enthalpy in products retained at the FTIR.**

effluent Fourier transform infrared (FTIR) absorption spectroscopy (top) and total power in chemistry with the input power (bottom). The total CO production is obtained by summing the rates of CO-producing and -consuming reactions in Figure 3. The total power consumed in chemical reactions is obtained the same way, but considering the enthalpy change of a reaction. The calculated power should be within the yellow area of Figure 4, the boundaries of which are given by the 1 kW input power and the power retained in stable products in the effluent, which reflects the true efficiency.



https://doi.org/10.1021/acsenergylett.1c01206
ACS Energy Lett. 2021, 6, 2876−2881

The rates obtained with the Butylkin data set overestimate CO production consistently and show, even beyond the error margins, a power consumption above 1000 W in the 120 mbar conditions. The Kozak and GRI-MECH schemes are similar in terms of CO production and power, although with the Kozak scheme, CO production from reaction R3 exceeds that of reaction R1 at 120 mbar. This gives the Kozak scheme a physically unfeasible negative O atom production rate: more O is consumed than produced. On the basis of these considerations, we recommend using GRI-MECH rate constants but also stress that a new evaluation of $CO_2$ rate constants at high temperature is necessary.

According to the results of Figure 3 and the GRI-MECH scheme, 68% of all O atoms are lost in O + $CO_2$ association, thereby producing 45% of all CO in the conditions of Figure 1 (120 mbar, 10 slm, 1000 W). The other plasma conditions show similarly high values. The apparent importance of this reaction forces a redefinition of the thermal efficiency limit. The current 52% limit is based on absolute quenching,[4,6,7] whereas we have experimentally shown superideal quenching, and the underlying O + $CO_2$ association reaction, to be a main $CO_2$ dissociation mechanism. Given this, the efficiency limit of thermal $CO_2$ splitting should be increased to 70%[6,8] to include the effective valorization of O atoms through superideal quenching.

The results also underline the opportunity to surpass the 50% efficiency via optimization of residence times in both core and periphery. Just outside the plasma core, with temperatures decreasing, competing reaction kinetics can lead to (un)-favorable utilization of the atomic oxygen. If the temperature falls below 2000 K and cooling is very fast, atomic O will preferentially recombine to $O_2$. Conversely, if cooling is too slow, O + CO recombination would be favored.[6,10] The optimal temperature for preferential super ideal quenching is 3000 K, where the predicted thermal equilibrium composition is primarily composed of CO and $O_2$. Therefore, to gain maximum utility from superideal quenching, the hot core of the plasma—the predominant source of atomic oxygen—should be surrounded by a cloak of gas maintained at 3000 K; this would create favorable reaction conditions and allow sufficient time for the relatively slow O + $CO_2$ reaction to occur.

In conclusion, we show that the high energy efficiency of the $CO_2$ microwave plasma is predominantly explained by thermal chemistry occurring within the plasma core, alongside a chemical nonequilibrium that facilitates superideal quenching of atomic oxygen. Steep temperature gradients drive fast core−periphery transport and mixing, thereby minimizing CO losses and optimizing O-utilization. Additionally, we find no evidence of a vibrational−translational nonequilibrium. This work therefore challenges the prevailing hypothesis that the vibrational dissociation mechanism is responsible for the reported high performance.

Further reactor engineering can improve efficiency by increasing the chemical nonequilibrium surrounding the core. This increases CO formation outside the core through superideal quenching of oxygen atoms. Reaching this superideally quenched system requires precise control over temperature and residence time but opens a window to boost $CO_2$ reduction efficiency to 70%.

## ■ ASSOCIATED CONTENT

### Supporting Information

The Supporting Information is available free of charge at https://pubs.acs.org/doi/10.1021/acsenergylett.1c01206.

Experimental details, comparison of thermal chemistry sets, spectral analysis, error analysis, additional results of rotational and vibrational Raman scattering, replacement frequencies, and chemical nonequilibrium (PDF)

## ■ AUTHOR INFORMATION


### Corresponding Author

**Gerard van Rooij** − *DIFFER, 5612AJ Eindhoven, The Netherlands; Faculty of Science and Engineering, Maastricht University, 6229 GS Maastricht, The Netherlands*; Email: g.vanrooij@maastrichtuniversity.nl

### Authors

**Alex van de Steeg** − *DIFFER, 5612AJ Eindhoven, The Netherlands*; orcid.org/0000-0002-2976-7905

**Pedro Viegas** − *DIFFER, 5612AJ Eindhoven, The Netherlands; Department of Physical Electronics, Faculty of Science, Masaryk University, 611 37 Brno, Czech Republic*

**Ana Silva** − *DIFFER, 5612AJ Eindhoven, The Netherlands*

**Tom Butterworth** − *Faculty of Science and Engineering, Maastricht University, 6229 GS Maastricht, The Netherlands*

**Alexander van Bavel** − *Shell Global Solutions International B.V., Amsterdam 1031 HW, The Netherlands*

**Joost Smits** − *Shell Global Solutions International B.V., Amsterdam 1031 HW, The Netherlands*

**Paola Diomede** − *Faculty of Science and Engineering, Maastricht University, 6229 GS Maastricht, The Netherlands*

**Mauritius van de Sanden** − *DIFFER, 5612AJ Eindhoven, The Netherlands*; orcid.org/0000-0002-4119-9971

Complete contact information is available at: https://pubs.acs.org/10.1021/acsenergylett.1c01206


### Notes

The authors declare no competing financial interest.

## ■ ACKNOWLEDGMENTS

This research received funding from The Netherlands Organization for Scientific Research (NWO) in the framework of the CO2-to-Products program with kind support from Shell and the ENW PPP Fund for the top sectors. We are grateful to E. Langereis for his support in the design of schematics.

## ■ REFERENCES


(1) Grim, R. G.; Huang, Z.; Guarnieri, M. T.; Ferrell, J. R.; Tao, L.; Schaidle, J. A. Transforming the Carbon Economy: Challenges and Opportunities in the Convergence of Low-Cost Electricity and Reductive $CO_2$ Utilization. *Energy Environ. Sci.* **2020**, *13* (2), 472−494.

(2) Graves, C.; Ebbesen, S. D.; Mogensen, M.; Lackner, K. S. Sustainable Hydrocarbon Fuels by Recycling $CO_2$ and $H_2O$ with Renewable or Nuclear Energy. *Renewable Sustainable Energy Rev.* **2011**, *15* (1), 1−23.

(3) Breyer, C.; Fasihi, M.; Bajamundi, C.; Creutzig, F. Direct Air Capture of $CO_2$: A Key Technology for Ambitious Climate Change Mitigation. *Joule* **2019**, *3* (9), 2053−2057.

(4) den Harder, N.; Van den Bekerom, D. C. M.; Al, R. S.; Graswinckel, M. F.; Palomares, J. M.; Peeters, F. J. J.; Ponduri, S.; Minea, T.; Bongers, W. A.; van de Sanden, M. C. M.; van Rooij, G. J. Homogeneous $CO_2$ Conversion by Microwave Plasma: Wave

Propagation and Diagnostics. *Plasma Processes Polym.* **2017**, *14* (6), 1600120.
(5) Bongers, W.; Bouwmeester, H.; Wolf, B.; Peeters, F.; Welzel, S.; Van Den Bekerom, D. C. M.; den Harder, N.; Goede, A.; Graswinckel, M.; Groen, P. W.; Kopecki, J.; Leins, M.; van Rooij, G.; Schulz, A.; Walker, M.; van de Sanden, M. C. M. Plasma-Driven Dissociation of $CO_2$ for Fuel Synthesis. *Plasma Processes Polym.* **2017**, *14* (6), 1600126.
(6) Wolf, A. J. J.; Peeters, F. J. J.; Groen, P. W. C.; Bongers, W. A.; Van De Sanden, M. C. M. $CO_2$ Conversion in Nonuniform Discharges: Disentangling Dissociation and Recombination Mechanisms. *J. Phys. Chem. C* **2020**, *124* (31), 16806−16819.
(7) Snoeckx, R.; Bogaerts, A. Plasma Technology-a Novel Solution for $CO_2$ Conversion? *Chem. Soc. Rev.* **2017**, *46* (19), 5805−5863.
(8) van den Bekerom, D. C. M.; Linares, J. M. P.; Verreycken, T.; van Veldhuizen, E. M.; Nijdam, S.; Berden, G.; Bongers, W. A.; van de Sanden, M. C. M.; van Rooij, G. J. The Importance of Thermal Dissociation in $CO_2$ Microwave Discharges Investigated by Power Pulsing and Rotational Raman Scattering. *Plasma Sources Sci. Technol.* **2019**, *28*, 055015.
(9) Fridman, A. *Plasma Chemistry*, 1st ed.; Cambridge University Press, 2008. DOI: 10.1192/bjp.111.479.1009-a.
(10) Vermeiren, V.; Bogaerts, A. Plasma-Based $CO_2$ Conversion: To Quench or Not to Quench? *J. Phys. Chem. C* **2020**, *124* (34), 18401−18415.
(11) Koelman, P.; Heijkers, S.; Tadayon Mousavi, S.; Graef, W.; Mihailova, D.; Kozak, T.; Bogaerts, A.; van Dijk, J. A Comprehensive Chemical Model for the Splitting of $CO_2$ in Non-Equilibrium Plasmas. *Plasma Processes Polym.* **2017**, *14*, 1600155.
(12) Butylkin, Y. P.; Zhivotov, V. K.; Krasheninnikov, E. G.; Krotov, M. F.; Rusanov, V. D.; Tarasov, Y. V.; Fridman, A. A. Dissociation of $CO_2$ by a Plasma-Chemical Process in a Nonequilibrium Microwave Discharge. *Sov. Phys. Technol. Phys.* **1981**, *26* (5), 555−558.
(13) Kozàk, T.; Bogaerts, A. Splitting of $CO_2$ by Vibrational Excitation in Non-Equilibrium Plasmas: A Reaction Kinetics Model. *Plasma Sources Sci. Technol.* **2014**, *23* (4), 045004.
(14) Soldatov, S.; Link, G.; Silberer, L.; Schmedt, C. M.; Carbone, E.; D'Isa, F.; Jelonnek, J.; Dittmeyer, R.; Navarrete, A. Time-Resolved Optical Emission Spectroscopy Reveals Nonequilibrium Conditions for $CO_2$ Splitting in Atmospheric Plasma Sustained with Ultrafast Microwave Pulsation. *ACS Energy Lett.* **2021**, *6* (1), 124−130.
(15) Pietanza, L. D.; Colonna, G.; D'Ammando, G.; Laricchiuta, A.; Capitelli, M. Non Equilibrium Vibrational Assisted Dissociation and Ionization Mechanisms in Cold $CO_2$ Plasmas. *Chem. Phys.* **2016**, *468*, 44−52.
(16) van den Bekerom, D.; van de Steeg, A.; Van de Sanden, M. C. M.; Van Rooij, G. J. Mode Resolved Heating Dynamics in Pulsed Microwave $CO_2$ Plasma from Laser Raman Scattering. *J. Phys. D: Appl. Phys.* **2020**, *53* (5), 054002.
(17) van de Steeg, A.; Butterworth, T.; van den Bekerom, D.; Silva, A.; van de Sanden, M. C. M.; van Rooij, G. Plasma Activation of $N_2$, $CH_4$ and $CO_2$: An Assessment of the Vibrational Non-Equilibrium Time Window. *Plasma Sources Sci. Technol.* **2020**, *29*, 115001.
(18) Klarenaar, B. L. M.; Morillo-Candas, A. S.; Grofulović, M.; Van De Sanden, M. C. M.; Engeln, R.; Guaitella, O. Excitation and Relaxation of the Asymmetric Stretch Mode of $CO_2$ in a Pulsed Glow Discharge. *Plasma Sources Sci. Technol.* **2019**, *28* (3), 035011.
(19) Viegas, P.; Vialetto, L.; Wolf, A. J.; Peeters, F.; Groen, P. W. C.; Righart, T. W. H.; Bongers, W.; Van de Sanden, M. C. M.; Diomede, P. Insight into Contraction Dynamics of Microwave Plasmas for $CO_2$ Conversion from Plasma Chemistry Modelling. *Plasma Sources Sci. Technol.* **2020**, *29*, 105014.
(20) Sun, H.; Lee, J.; Do, H.; Im, S. K.; Soo Bak, M. Experimental and Numerical Studies on Carbon Dioxide Decomposition in Atmospheric Electrodeless Microwave Plasmas. *J. Appl. Phys.* **2017**, *122* (3), 033303.
(21) Van de Steeg, A. W.; Vialetto, L.; Silva, A. F.; Peeters, F. J. J.; Van den Bekerom, D. C. M.; Gatti, N.; Diomede, P.; Van de Sanden, M. C. M.; Van Rooij, G. J. Revisiting Spontaneous Raman Scattering for Direct Oxygen Atom Quantification. *Opt. Lett.* **2021**, *46* (9), 2172−2175.
(22) Butylkin, Y. P.; Grinenko, A. A.; Levitskii, A. A.; Polak, L. S.; Rytova, N. M.; Slovetskii, D. I. Mathematical Modeling of the Kinetics of the Thermal Decomposition of Carbon Dioxide in an Electric Arc Discharge and Quenching of the Product. *Sov. Phys., High Energy Chem.* **1979**, *13* (6), 545−551.
(23) Smith, G. P.; Golden, D. M.; Frenklach, M.; Moriarty, N. W.; Eiteneer, B.; Goldenberg, M.; Bowman, C. T.; Hanson, R. K.; Song, S.; Gardiner, W. C. J.; Lissianski, V. V.; Qin, Z. Gri-Mech. http://combustion.berkeley.edu/gri-mech/overview.html.
(24) Pietanza, L. D.; Colonna, G.; Capitelli, M. Kinetics versus Thermodynamics on $CO_2$ Dissociation in High Temperature Microwave Discharges. *Plasma Sources Sci. Technol.* **2020**, *29* (3), 035022.
(25) Wolf, A. J.; Righart, T. W. H.; Peeters, F.; Groen, P. W. C.; Van de Sanden, M. C. M.; Bongers, W. Characterization of the $CO_2$ Microwave Plasma Based on the Phenomenon of Skin Depth-Limited Contraction. *Plasma Sources Sci. Technol.* **2019**, *28*, 115022.
(26) D'Isa, F. A.; Carbone, E. A. D.; Hecimovic, A.; Fantz, U. Performance Analysis of a 2.45 GHz Microwave Plasma Torch for $CO_2$. *Plasma Sources Sci. Technol.* **2020**, *29*, 105009.
(27) Kotov, V.; Koelman, P. M. J. Plug Flow Reactor Model of the Plasma Chemical Conversion of $CO_2$. *Plasma Sources Sci. Technol.* **2019**, *28* (9), 095002.
(28) Wolf, A. J.; Righart, T. W. H.; Peeters, F. J. J.; Bongers, W. A.; Van De Sanden, M. C. M. Implications of Thermo-Chemical Instability on the Contracted Modes in $CO_2$ Microwave Plasmas. *Plasma Sources Sci. Technol.* **2020**, *29* (2), 025005.


https://doi.org/10.1021/acsenergylett.1c01206
*ACS Energy Lett.* 2021, 6, 2876−2881